NMR Imaging of Diffusion Processes in Polymers: Measurement of the Spatial Dependence of Solvent Mobility in Partially Swollen PMMA Rods

L. A. Weisenberger and J. L. Koenig*

Department of Macromolecular Science, Case Western Reserve University, Cleveland, Ohio 44106. *Received May 23, 1989; Revised Manuscript Received September 19, 1989*

ABSTRACT: NMR imaging is used to study the spatial distribution of NMR relaxation times and self-diffusion coefficients of organic solvents in partially swollen PMMA. The solvents diffuse with Case II characteristics. T_1s, T_2s, and self-diffusion coefficients are measured as a function of distance from the glassy core of the polymer. The results show decreases in all three parameters toward the glassy core despite the fact that the concentration of solvent is constant throughout the swollen region. This indicates that the solvent motions are decreasing in that direction. A conceptual model is proposed which attributes the decrease in solvent relaxation times to the decrease in mobility of the polymer chains toward the core. This decrease is a result of the polymer chains being effectively fixed at the interface between the swollen and glassy regions of the sample. Several methods for acquiring images for determining T_1s, T_2s, and self-diffusion coefficients are demonstrated and compared.

Introduction

Solvent diffusion in polymers is important to the physical properties of materials from processing to end use and self-life. Many aspects of diffusion in polymers have been studied by using indirect methods such as gravimetric analysis and optical microscopy. A new technique is available to directly investigate the behavior of solvents imbibed in a polymer. Nuclear magnetic resonance (NMR) imaging is a modification of NMR spectroscopic techniques which uses linear magnetic field gradients to spatially encode the spins according to frequency and phase. The details of NMR imaging are described in several reviews,[1-10] and the application of NMR imaging to diffusion in polymers is discussed in several recent papers.[11-16] NMR imaging has the advantage that it does not disturb the diffusion process unlike most other techniques which require stopping the diffusion process and destroying the sample. Another advantage of NMR imaging is that almot any information available from NMR spectroscopy may be obtained on a spatial basis by using NMR imaging.

NMR imaging is typically used for examining structures in materials in a noninvasive manner by detecting the mobile protons of solvent molecules. Since NMR imaging is sensitive to mobile protons, it is an excellent tool for studying solvent diffusion in polymers. One aspect of NMR imaging that has yet to be fully exploited is that most information available through NMR spectroscopy is available on a spatial basis with NMR imaging. In particular for heterogeneous samples, the spatial distributions of spin–lattice, T_1, and spin–spin, T_2, relaxation times are obtainable. These parameters are important in determining the motions of the solvent molecules and the degree of interaction of the solvent molecules with their environment. In the case of diffusion into a polymer, the spatial distribution of T_1s and T_2s indicates the influence of the polymer matrix on the mobility of the solvent molecules.

Self-diffusion coefficients provide important information concerning the extent of the translation of solvent molecules in their environment. This information is easily interpreted in terms of molecular organization and phase structure. The self-diffusion coefficients are sensitive to structural changes as well as binding and association phenomena. Current theories on Case II diffusion assume that the self-diffusion of the solvent imbibed in the polymer is much faster than the actual diffusion of the solvent at the interface between the swollen polymer and the glassy polymer.[17-19]

Many glassy polymers exhibit diffusion behavior differing from normal Fickian diffusion. Case II diffusion is one extreme of diffusion phenomena exhibited by polymers and is characterized by (1) a sharp increase in solvent concentration at the interface between the swollen and nonswollen regions of the polymer, (2) this sharp front moves through the glassy polymer at a rate that is linear with time, and (3) the solvent concentration is constant throughout the swollen region. Case II diffusion is typically observed in polymers below T_g especially with solvents with high activities. These unique features of Case II diffusion make such systems excellent to study using NMR imaging because the concentration profile is simple and observation of the solvent advance is easier.

This paper describes the measurement of solvent T_1s, T_2s, and self-diffusion coefficients for solvents in poly(methyl methacrylate) (PMMA) as a function of position. Structural features for the swollen region near the glassy core are proposed and their ramifications on current case II theories are discussed.

Experimental Section

The Spin-Echo Imaging Pulse Sequence. Several techniques are available to measure solvent T_1s, T_2s, and self-diffusion coefficients in PMMA. The typical imaging pulse sequence is based on the spin-echo pulse sequences of Carr and Purcell[20] and Meiboom and Gill.[21] Figure 1 is the spin-echo imaging pulse sequence. The 90° rf pulse tips the magnetization into the x'–y' plane where it begins dephasing. The 180° rf pulse is applied after a time, τ, forcing the magnetization to refocus at a time 2τ (also known as the echo time, TE) after the 90° rf pulse at which time the data are collected. The frequency-encoding gradient, GX, causes the spins to precess at different frequencies depending on their position in the static magnetic field, H_0. The phase-encoding gradient, GY, is orthogonal to GX. Varying the intensity of GY causes the spins to dephase at different rates providing the second dimension of a two dimensional image. The slice selection gradient, GZ, and the Gaussian-shaped 90° rf pulse determine the position and thickness of the region of interest. The data are Fourier transformed in two dimensions

0024-9297/90/2223-2445$02.50/0

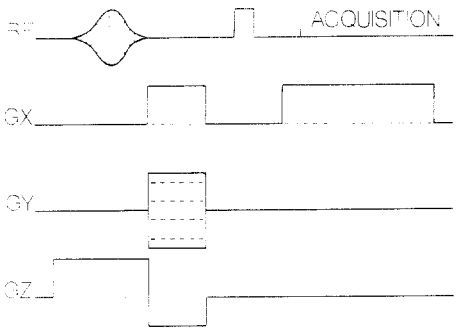

Figure 1. The timing diagram for the spin-echo imaging pulse sequence.

to produce the image of the selected slice.

Measurements of Spin–Lattice Relaxations. Series Method. The spin-echo sequence is used to determine both T_1s and T_2s. T_1s are determined collecting several images with different repetition times, TRs. The magnetization, M_0, is attenuated due to saturation according to eq 1. Thus, spins with

$$M = M_0(1 - \exp(-\mathrm{TR}/T_1)) \tag{1}$$

long T_1s are more saturated with shorter TRs, and their signals are more attenuated. Images are acquired at the same TE but with varying TRs. Curve-fitting software called TIGAUSS fits the series of images to eq 1 on a pixel-by-pixel basis using a nonlinear least-squares method. The contrast of the resulting image is based solely on the T_1s of the system providing a visual representation of the spatial distribution of T_1s.

Inversion Recovery Method. T_1s are also studied by using the T_1 inversion recovery imaging pulse sequence shown in Figure 2. A nonselective 180° rf pulse inverts the spins along H_0. The delay, τ, allows them to relax toward equilibrium. The selective 90° rf pulse brings the spins into the x'–y' plane for signal acquisition. The remainder of the sequence is equivalent to that in Figure 1 and contains the gradients necessary to form a two-dimensional image. Phase-sensitive images images provide greater contrast between fast and slow recovering species over magnitude images. They also provide the ability of isolating one component of a two component system by using the proper delay time and nulling the appropriate signal.

The signal from the inversion recovery experiment is determined by eq 2. The T_1s may be determined from the null point of the inversion recovery process according to eq 3. Although it is more appropriate to fit the several images on a pixel-by-pixel basis to eq 2, eq 3 is a faster way of getting T_1 information since fewer images are needed.

$$M = M_0(1 - 2\exp(-\tau/T_1)) \tag{2}$$

$$T_1 = \tau/(\ln 2) \tag{3}$$

Measurements of Spin–Spin Relaxations. Series Method. Similar to the series method for T_1s, the T_2s of the system are measured by varying TE with TR constant. The signal attenuation goes as eq 4. Like the T_1s, the T_2s are calculated on a pixel-by-pixel basis using the program T2EXP producing an image with contrast due only to the T_2s of the system. The spins with shorter T_2s are represented by lower intensities than those with longer T_2s.

$$M = M_0 \exp(-\mathrm{TE}/T_2) \tag{4}$$

Multiecho Method. T_2 images are also generated by using a multiecho version of the spin-echo experiment as shown in Figure 3. A nonselective 180° rf pulse is applied at a time, τ, after the acquisition which produces a second echo at time 2τ after the second 180° rf pulse. The total echo time for the second echo is 2TE. A second incremented gradient in the y direction after acquisition is used to rephase the spins before the next 180° rf pulse. The cycle is repeated until the desired number of echoes are acquired. The echo time for the nth echo in nTE. This allows the total experiment time to be reduced by the total number of different echoes acquired since all echoes are collected within one delay time rather than one echo per delay. The echoes that resulted from each echo time are separated and then individually Fourier transformed in two dimensions.

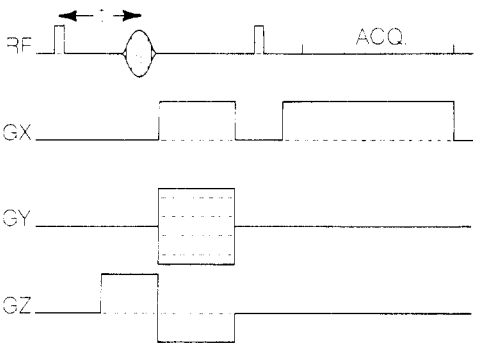

Figure 2. The timing diagram for the T_1 inversion recovery imaging pulse sequence.

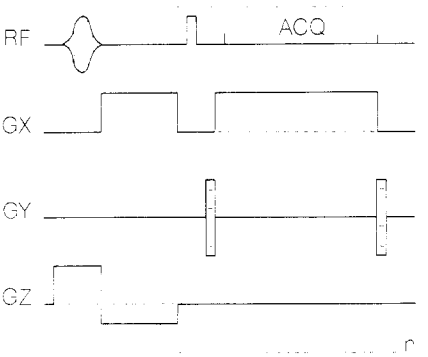

Figure 3. The timing diagram for the multiecho imaging pulse sequence.

Figure 4. The timing diagram for the pulsed gradient spin-echo pulse sequence for determining self-diffusion coefficients.

Measurements of Self-Diffusion Coefficients. Spin-Echo Techniques. The measurement of self-diffusion coefficients in NMR spectroscopy is accomplished by using the pulsed gradient spin-echo (PGSE) pulse sequence refined by Stejskal and Tanner.[22] Figure 4 is the timing diagram for the PGSE experiment. The rf pulse timing is a spin-echo experiment similar to those developed by Carr and Purcell[20] and Meiboom and Gill.[21] The first gradient pulse causes the spins to dephase at a spatially dependent rate. After the 180° rf pulse, the second gradient causes the spins to refocus at the same spatially dependent rate. Under static conditions, all of the spins refocus at the correct time and generate an echo whose intensity is only attenuated by spin–spin effects. However, all solvent molecules are subject to Brownian motions and move into regions of different effective fields. The result is that the spins do not refocus correctly and the echo is attenuated according to eq 5. The first exponential term is the attenuation due to the transverse relaxation, T_2, occurring during TE. The second exponential term accounts for the attenuation due to diffusion in the presence of a gradient pulse, G, which is on for a duration, δ. β is the combination of the duration time of the gradient pulses, δ, and the interval between them, Δ, as given by eq 6. For spectra collected at the same TE, the first term cancels. A plot of the natural log of the normalized signal versus $\gamma^2G^2\beta$ is linear with the slope being the self-diffusion coefficient, D.

$$M = M_0 \exp\left(-\frac{\mathrm{TE}}{T_2}\right) \exp(-\gamma^2G^2\beta D) \tag{5}$$

$$\beta = \delta^2\left(\Delta - \frac{\delta}{3}\right) \quad (6)$$

The imaging sequence in Figure 1 is easily adapted to the PGSE technique by adding two additional gradients in the x direction.[23] The equations are the same as the spectroscopic version, and the read gradients have little effect if they are much smaller than the motion probing gradients. However, this pulsed gradient imaging technique suffers from two restrictions. In order to attenuate the signal sufficiently on slow moving solvents, either the motion probing gradients or the interval between them must be large. Large gradients (i.e. >100 G cm^{-1}) are difficult to achieve on superconducting magnets without severe eddy current problems. And from eq 5, the interval between the pulsed gradients that allows the spins to diffuse forces TE to be longer when investigating slow moving species. Therefore, signals from spins with short T_2s are attenuated and may be undetectable.

Stimulated-Echo Techniques. An alternative approach is to use stimulated echoes. Figure 5 is the timing diagram for the stimulated echo acquisition mode (STEAM) diffusion imaging pulse sequence.[24,25] The STEAM pulse sequence uses three 90° rf pulses to generate a stimulated echo. The difference between STEAM and a spin-echo sequence is that the second 90° rf pulse stores magnetization along the z direction and the third 90° rf pulse recovers the magnetization. Since the magnetization is stored in the z direction, the time between the last two 90° rf pulses permits the spins to diffuse with loss of signal due to spin–lattice rather than spin–spin effects. Since T_1s are generally longer than T_2s, longer intervals and weaker gradients are used to see the effects of slow diffusion with minimal effects from T_2 relaxations.

The signal is determined according to eq 7 which differs from eq 1 by the exponential term containing the effects of T_1 relaxation occurring during the storage interval, TI.[26] While the T_2

$$M = M_0 \exp\left(-\frac{\mathrm{TE}}{T_2}\right) \exp\left(-\frac{\mathrm{TI}}{T_1}\right) \exp(-\gamma^2 G^2 \beta D) \quad (7)$$

effects still contribute to the signal attenuation, any increase in Δ can be added to TI instead of TE. In this situation, signal attenuation due to relaxation is considerably less. For example given a T_1 of 100 ms and a T_2 of 20 ms, a 10-ms increase in Δ results in a 10% further attenuation by T_1s when added to TI but a 40% further attenuation by the T_2s when added to TE.

Equipment and Materials. The imaging system is based on the Bruker MSL 300 spectrometer with microimaging. The gradients are generated by using gradient coils inside of the probe. Gradient amplification is achieved with NAD amplifiers and pre- and post-emphasis are used with all gradients. Gradient strength for the read direction is typically 6 G cm^{-1} producing a resolution of about 90 μm. Gradient strength of the motion probing gradients range from 3.5 to 13.9 G cm^{-1} for the acetone system and from 13.9 to 68.8 G cm^{-1} for the methanol system.

Gaussian-shaped rf pulses are generated by using a selective excitation unit and are 1 ms long producing a 2-mm slice thickness. The nonselective 90° rf pulses are about 40 μs. The echo times used in the multiecho sequence are multiples of 5.25 ms. The repetition time, TR, used is 3 s. The echo times used for the series method are 8, 12, 16, 20, and 24 ms with a repetition time of 10 s. The repetition times used for T_1 determination by the series method are 1, 2, 4, 6, 8, and 10 s with an echo time of 8 ms. The stimulated-echo version of the diffusion pulse sequence uses a TE of 7.5 ms, a TI of 103 ms, and a TR of 3 s. Four echoes of each phase-encoding step are coadded by using cyclops phase cycling. The data set is 256 points spread across 62.5 kHz with 256 phase-encoding steps.

Images are transferred from the Aspect 3000 computer of the imaging system to a MicroVax II via Ethernet communications. They are then processed by using software written in Fortran 77 by J. Liu of this group. Processing includes noise-filtering and color-scale manipulation. T_1 and T_2 images are generated from several images using T1GAUSS and T2EXP, respectively. These programs are nonlinear least-squares fits on a pixel-by-pixel basis to the equations given previously in this paper. The averages and standard deviations for each relaxation parameter were established by sampling the region of interest of the reconstructed images.

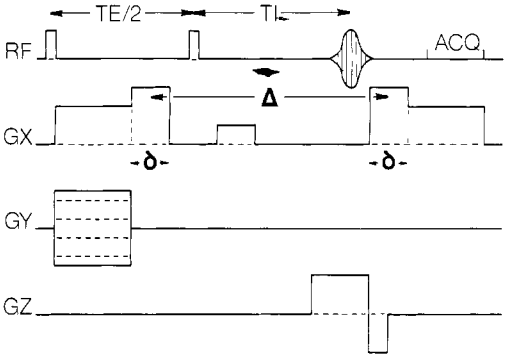

Figure 5. The timing diagram for the pulsed gradient stimulated-echo imaging pulse sequence for determining self-diffusion coefficients spatially.

The self-diffusion coefficient images are generated by using the magnitude images collected and T2EXP. The images are fit to eq 8 as a function of the gradient attenuation factor, d, where $d = \gamma^2 G^2 \beta$. This generates an image based on the dummy

$$I = I_0 \exp(-d/B) \quad (8)$$

variable, B. The inverse of the image is taken to generate the self-diffusion coefficient image based on D according to eq 7. It is possible to use this procedure since only the motion probing gradients are changed. The remainder of the attenuation terms in eq 7 cancel in the fitting procedure.

The samples are 12.7-mm lightly cross-linked PMMA rods from Commercial Plastics and Supplies Corp., Cleveland, OH. The methanol is deuterated at the hydroxy position (99.5%) and is used as received from Aldrich Chemical. The acetone is lab grade from Fischer Scientific. Each sample is submersed in the appropriate solvent at 30 °C until the desired swelling is achieved, 20 days for the methanol samples, and 12 h for the acetone samples. Each sample is sealed in a vial with only enough bulk solvent to cover the bottom of the vial. Although this stops the diffusion process, the desorption of the solvent is slow enough in the presences of the methanol vapor to maintain the solvent concentration distribution in the polymer long enough for the images to be acquired. The removal of the solvent permits lowering the receiver gain to the level of the imbibed solvent rather than the more intense bulk solvent, thus substantially increasing the signal-to-noise ratio of the imbibed regions.

A spin-echo image was also acquired by using perdeuterated methanol to determine the signal contribution from the protons of the swollen PMMA under the same experimental conditions used for the hydroxy deuterated samples. No signal from the protons of the polymer was apparent after four acquisitions. Apparently, the T_2s of these protons are still too short to be detectable at this echo time.

Results

Figure 6 contains a series of images of methanol in PMMA at different echo times from the multiecho experiment. The intensities are represented here by colors with red being the highest intensity and dark blue being the lowest. The T_2 attenuation of the intensity is more apparent for the longer echo times. Figure 7 is the calculated T_2 image from the images in Figure 6. In this case red represents the longer T_2s and dark blue the shorter. Figure 8 is a profile of the image in Figure 7 showing an almost linear decrease of T_2s to the center core. Figures 7 and 8 show a substantial decrese in T_2s from the outer edge of the sample to the glassy core.

Figure 9 is an inversion recovery image of methanol in PMMA with a τ of 100 ms. The bright regions (yellow,

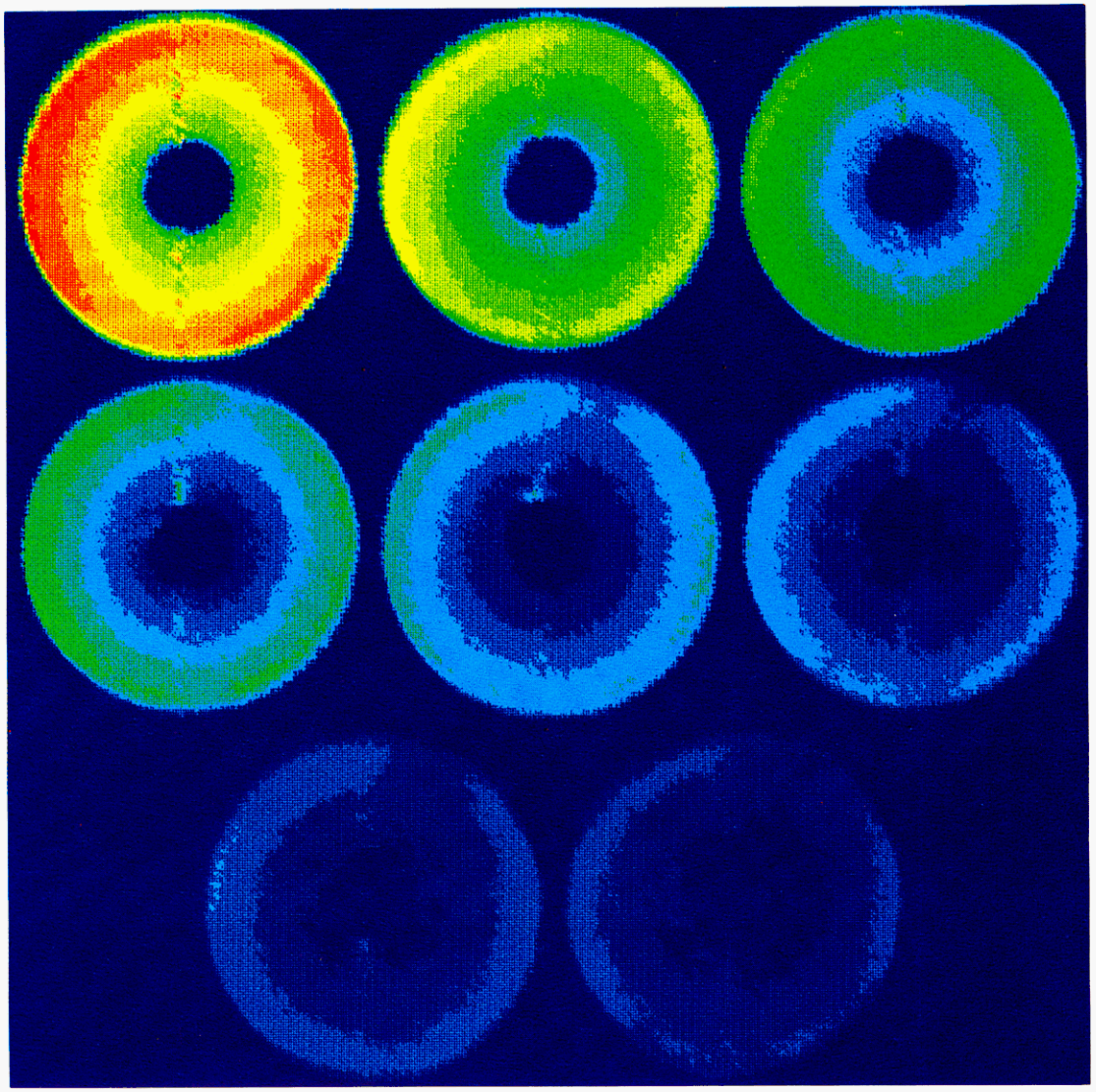

Figure 6. Eight images acquired with the multi-echo pulse sequence of a 12.7-mm PMMA rod swollen in methanol at 30 °C. TE (reading from the top left to lower right) (A) 5.25, (B) 10.50, (C) 15.75, (D) 21.00, (E) 26.25, (F) 31.50, (G) 36.75, and (H) 42.00 ms.

orange, and red in increasing order) are positive values, and the dark regions (light blue through dark blue in decreasing order) are negative values. The nulled regions are where the intensities are the same shade of green as the area surrounding the rod. Figure 10 is a profile across the image in Figure 9. The poor signal-to-noise in Figure 10 is a result of being near the null point for most of the regions in the sample. Both figures indicate that the T_1s are smaller toward the glassy core of the polymer. The area at the outside edge of the rod appears lighter than the background indicating a positive intensity and a short T_1. This is possibly due to the influence of the paramagnetic oxygen in the surrounding methanol vapor.

Table I contains the T_1s and T_2s for the various techniques and different locations in the samples. Table I indicates that the methanol relaxation times near the core are 40–66% lower than those near the polymer surface. The acetone T_1s only decrease by 16% between the outer and inner regions, but the acetone T_2s decrease by 66% from the outer to the inner regions.

Figure 11 is a series of images of methanol in PMMA taken at different gradient strengths. Each successive image is the result of a more intense motion probing gradient. The first image shows a more intense signal on the outer regions of the rod with the intensity decreasing toward the core. The decrease is due to the T_2 attenuation as described in a recent paper.[16] This does not affect the calculation of the self-diffusion coefficients since the T_2s for each region remain constant and since neither TE nor TI are varied in the STEAM diffusion pulse sequence. Figure 12 is the calculated self-diffusion coefficient image generated from those images in Figure 11. Figure 12 shows a range of coefficients. The region within 100 μm of the glassy core exhibits a self-diffusion coefficient of $(3.2 \pm 0.9) \times 10^{-7}$ cm^2 s^{-1}. The outer region of the swollen polymer exhibits an self-diffusion coefficient of $(9.2 \pm 0.9) \times 10^{-7}$ cm^2 s^{-1}. The self-diffusion coefficient image has more noise than the original images. The pulse sequences described previously use motion probing gradients in only one direction. Since the solvent self-diffusion is a random process, the spins travel in all directions. Those spins traveling in a direction other than that of the motion probing gradient cause the wide variation in pixel intensities.

Figure 13 is the plot of natural log of intensities from Figure 11 against the gradient attenuation factor, d, for two regions in the sample, one near the core and one near the surface. The line through each set of data is the least-squares fit to eq 9 where I is the intensity, d is the gra-

$$\ln (I) = -Dd + A \tag{9}$$

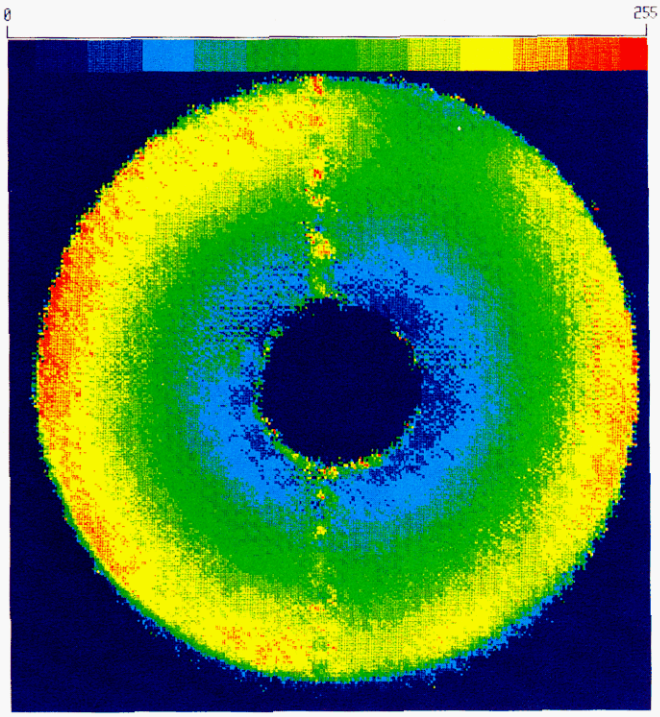

Figure 7. The T_2 image calculated from the images in Figure 4. The color scale at the top of the image represents T_2s ranging from A (red), 7 ms, to B (dark blue), 24 ms.

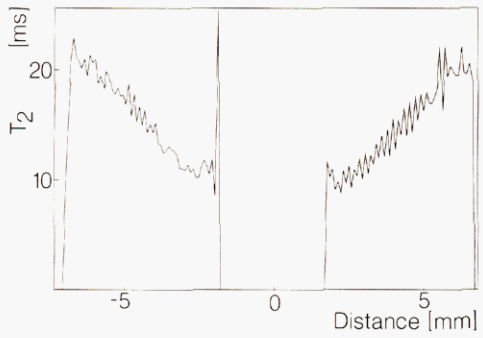

Figure 8. The profile through the center of the T_2 image in Figure 7.

dient attenuation factor that accounts for the gradient strength, durations, and the interval between them, D is the self-diffusion coefficient, and A is the intercept.

Figure 14 is the calculated self-diffusion coefficient image of acetone in PMMA. This image also shows that the self-diffusion coefficients are smaller toward the glassy core. The self-diffusion coefficient image shows that the self-diffusion coefficients from 1.8 mm from the glassy core out to the surface of the rod are constant. The self-diffusion coefficient within 100 μm of the core is $(2.1 \pm 0.9) \times 10^{-5}$ cm^2 s^{-1}. The self-diffusion coefficient in the regions where equilibrium is established the self-diffusion coefficient is $(3.2 \pm 0.9) \times 10^{-5}$ cm^2 s^{-1}. Figure 15 is the profile of the image in Figure 14.

Discussion

The characteristics of Case II diffusion are extensively reported throughout the literature.[14-19,27-30] Two static characteristics concern the shape of the concentration profile of the solvent in the polymer. The first is the solvent concentration goes from zero in the glassy core to a finite value over a short distance producing a nearly steplike profile at the glass–rubber interface. The second is the imbibed solvent concentration is constant throughout the swollen regions of the polymer. These

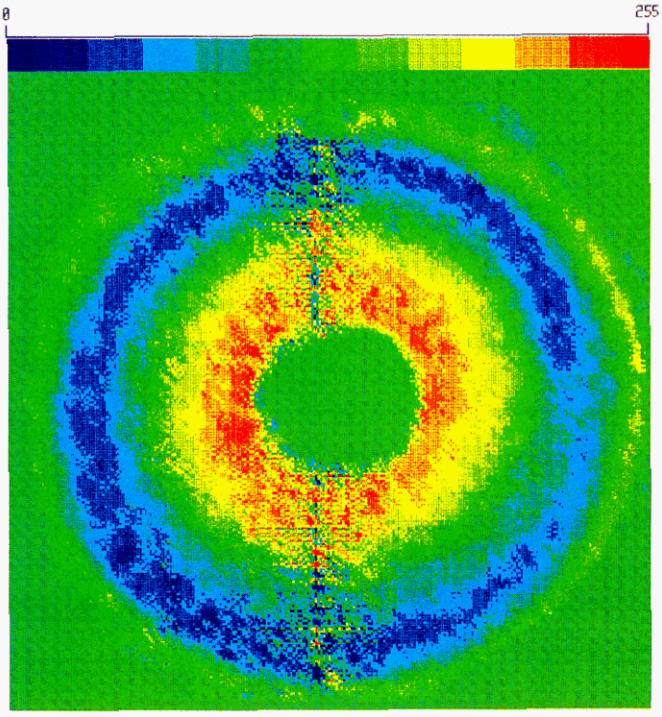

Figure 9. The T_1 inversion recovery image acquired with τ = 100 ms of a 12.7-mm PMMA rod swollen in methanol at 30 °C. The color scale is in arbitrary intensity units ranging from A (red), −0.10, to B (dark blue), 0.13.

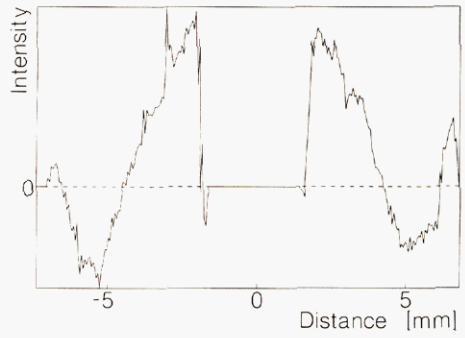

Figure 10. The intensity profile through the center of the image in Figure 9.

characteristics indicate that the volume fraction of solvent in the polymer is the same throughout the swollen regions of the sample including in the vicinity of the glassy polymer core and have been verified by several techniques including NMR imaging.[14-19,28-30]

Spatial T_1 and T_2 Measurements. NMR relaxation parameters have been a useful probe of molecular motions in polymers and other organic molecules. However, each correlation time represents the average value of the system with some distribution around that average. NMR imaging permits the determination of the spatial distribution of NMR relaxation times. This distribution provides information concerning the local motions of the system. In this case, the polymer is partially swollen with solvent and the spatial distributions of relaxation times reveal the interactions between the solvent, the polymer and the diffusion process.

The volume fraction of methanol in the polymer is constant from the polymer surface to the glassy core.[14-19,28-30] However, the methanol T_1s and T_2s decrease toward the glassy core. Since the volume available to the methanol molecules are the same from the surface to the core, the relaxation times should be constant throughout the region if no other interactions exist. The T_1s and T_2s change

Table I
NMR Relaxation Parameters for Solvents in PMMA Determined from the Techniques Discussed in the Text[a]

NMR parameter (technique)	sample (location)			
	MeOD (inner)	MeOD (outer)	acetone (inner)	acetone (outer)
T_2, ms (ME)	10.0 ± 0.8	19.8 ± 0.7	130 ± 50	380 ± 20
T_2, ms (S)	12 ± 1	18 ± 4		
T_1, s (S)	0.3 ± 0.1	0.5 ± 0.1		
T_1, s (IR)	0.08 ± 0.01	0.17 ± 0.01	2.0 ± 0.1	2.4 ± 0.1

[a] Abbreviations: inner = 200 μm from the glassy polymer core; outer = 500 μm from polymer surface; ME = multiecho experiment; S = series technique; IR = inversion recovery experiment.

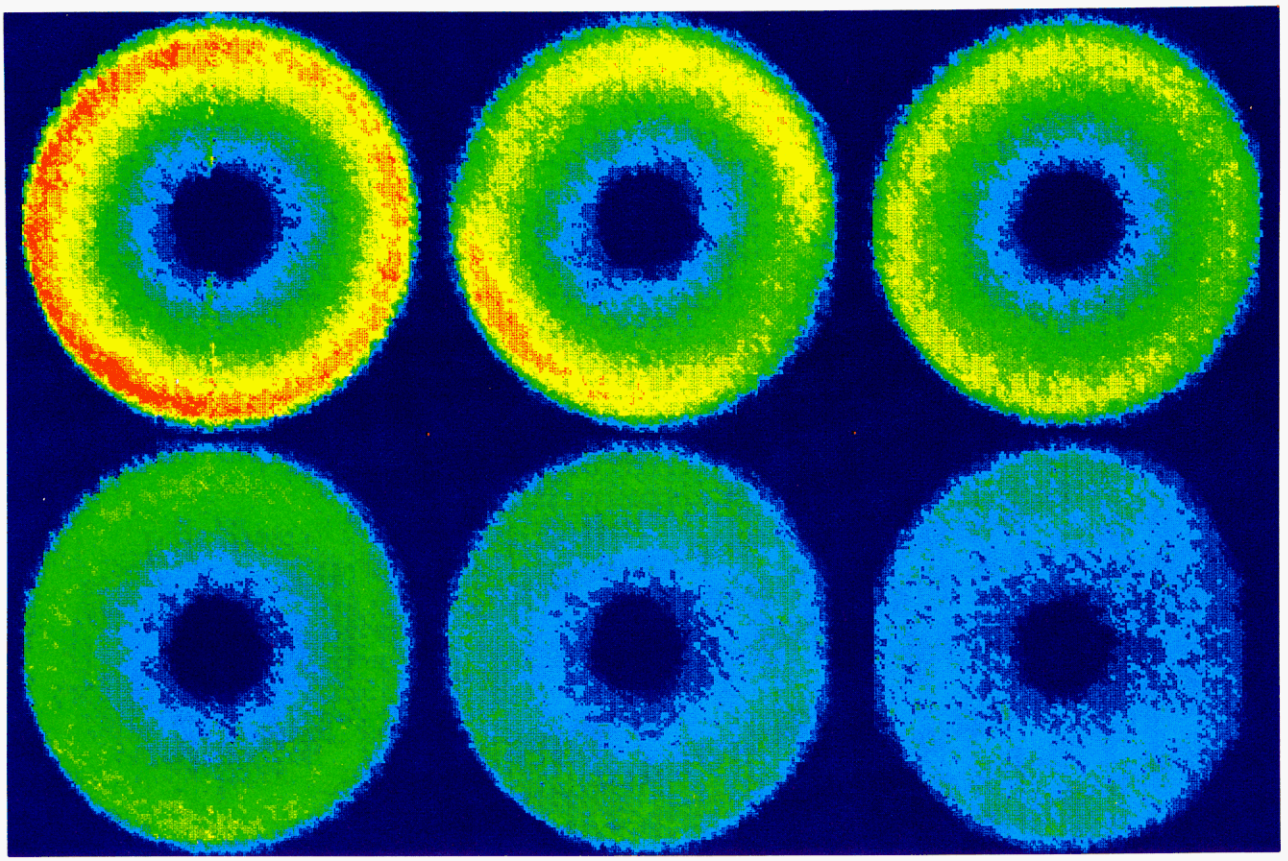

Figure 11. Six images of methanol in a PMMA rod acquired with the stimulated-echo imaging pulse sequence at different gradient strengths (reading from upper left to lower right); (A) 0, (B) 13.9, (C) 27.6, (D) 41.4, (E) 55.1, and (F) 68.8 G/cm.

substantially from the surface to the core indicating that a physical effect other than just free volume is affecting the mobility of the solvent. Infrared spectroscopy studies[31] indicate that no spectroscopically detectable chemical interactions occur between the polymer and the solvent, so that the controlling interaction must be physical.

Two effects contributing to the differences between bulk solvent and imbibed solvent diffusion properties are the obstruction effect and the hydrodynamic drag.[32,33] The obstruction effect is the presence of the polymer forcing the solvent to take an extended pathway. Hydrodynamic drag is the localized slowing of solvent molecules near a polymer chain. Both of these factors were studied by other groups on fully swollen gels where an equilibrium exists throughout the samples.[32,33]

The data presented here are from an intentionally anisotropic sample and the factors discussed above are inadequate to explain the decrease in T_1s and T_2s toward the center of the sample. A dynamic obstruction effect is more appropriate for this situation. The polymer core effectively fixes the position of the chains at the interface between the swollen and the glassy regions of the polymer. The polymer chain dynamics go from the usual anisotropic motions with a variety of frequencies and amplitudes to anisotropic motions with the frequencies and amplitudes dependent on the position along the polymer chain. Frequencies and amplitudes decrease toward the fixed point of the chain, i.e. the glassy core.

However, the solvent relaxation times are measured here not the polymer relaxation times. The polymer relaxation times are not available as a spatial image with current technology, since the shortest echo time that accommodates gradient switching is around 5 ms. The solvent relaxation times measured here are indicative of the motions of the polymer chains because of the hydrodynamic drag. Since the solution is highly concentrated, most solvent molecules are influenced by the hydrodynamic drag. So the two sets of motions, that of the polymer and of the solvent, must be cooperative, and the solvent relaxation times reflect the motions of the polymer chains. This is consistent with the findings of Blum et al.,[34] who show that the local segmental motions of the polymer are similar to the movement of the solvent molecules by comparing deuterium T_2s of the polymer backbone and solvent self-diffusion coefficients from NMR.

In polymers, the T_1 and T_2 data are sensitive to two different motional regimes. The T_1s are sensitive to megahertz motions which are typically short range and are

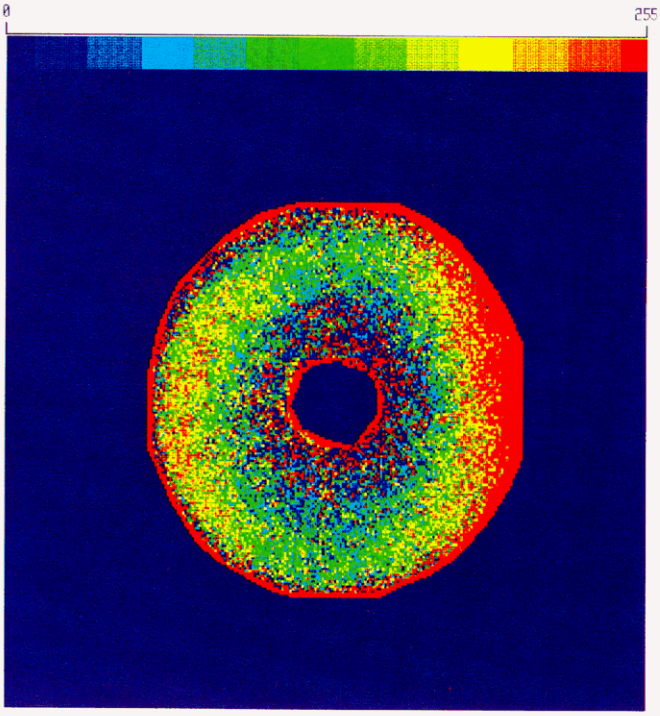

Figure 12. The self-diffusion coefficient image for methanol in PMMA calculated from the images in Figure 11. The color scale represents self-diffusion coefficients from A (red), 2×10^{-7} cm^2/s, to B (dark blue), 11×10^{-7} cm^2/s.

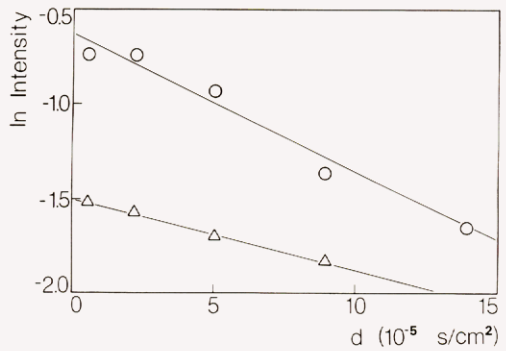

Figure 13. A plot of the natural log intensity versus the gradient attenuation factor, d, for a region near the glassy core (△) and a region near the surface (○).

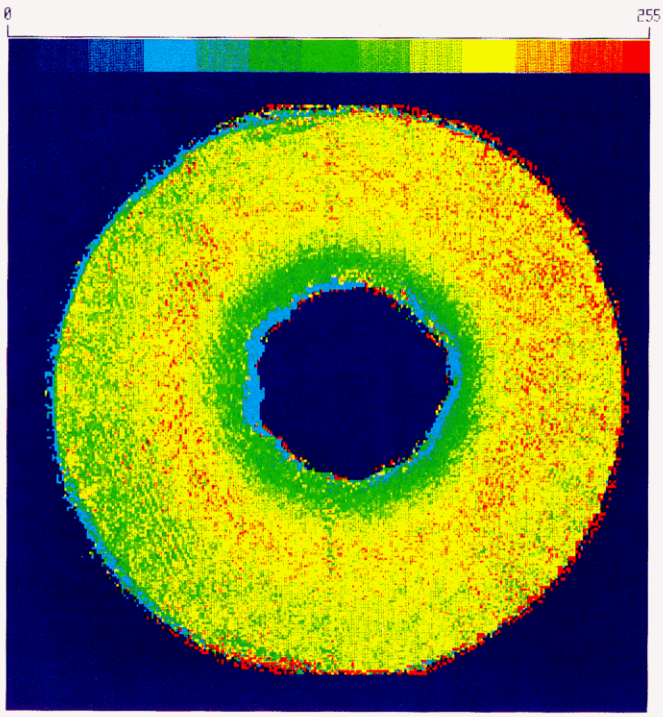

Figure 14. The self-diffusion coefficient image for acetone in PMMA calculated from four images acquired with gradient strengths from 3.5 to 13.9 G/cm. The color scale represents self-diffusion coefficients from A (red), 0 cm^2/s, to B (dark blue), 4×10^{-5} cm^2/s.

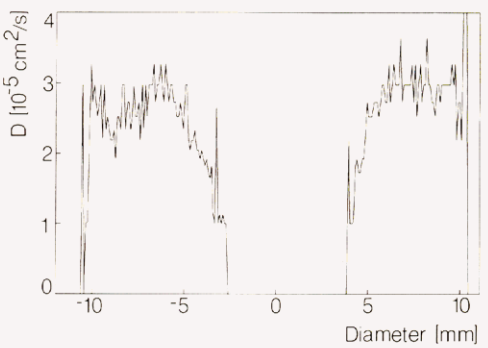

Figure 15. The profile from the self-diffusion coefficient image in Figure 14.

often side chain motions. The T_2s are sensitive to the longer range segmental motions of the polymer backbone. In solvents, the number of bonds over which interactions take place is much smaller and the T_1s and T_2s are usually similar in magnitude. The significant decrease in T_2s compared to T_1s indicates that the solvent is interacting with the polymer on a longer distance scale. This may indicate the influence of the network structure on the motions of the cross-linked polymer.

The acetone data represent a condition in which the solvent volume fraction is much higher than in the methanol case. The T_2s are significantly larger for acetone because of the greater free volume available to the solvent. The difference between the inner and outer T_2s is almost a factor of 3 rather than 2 seen in the methanol system. The acetone system also reaches a level of constant T_2s a few millimeters from the glassy core. The acetone system reaches a constant T_2 level, and the methanol system continues to change out to the surface. The difference between the two systems indicates that the acetone system has reached an ultimate motional state in the region of constant T_2 and the methanol system has not established this condition.

The distance over which the T_2s decrease in the methanol system is long compared to molecular distances. This sample is slightly cross-linked, and the decrease in T_2s from the surface to the core may reflect the structure of the network. A non-cross-linked sample may reach motional equilibrium a specific distance from the glassy core depending on the polymer molecular weight and the solvent temperature and activity.

The T_1s of the acetone system only decrease 17%. This is considerably less than the other measurements discussed. This is consistent with the dynamics of the T_1 measurements. The solvent volume fraction is considerably more than in the other cases, and the T_1s are sensitive to short-range motions. The solvent molecules are more influenced by the surrounding solvent molecules than by the presence and the motions of the polymer. The acetone T_1s are only moderately effected by the restricted motions of the polymer chains near the glassy core.

Self-Diffusion Coefficients. Since the volume fraction of solvent is constant, the free volume available for self-diffusion is also constant. This implies that the self-diffusion coefficient should be constant throughout the swollen region in the absence of other effects. Clearly from Figure 12, the methanol/PMMA system exhibits a distribution of self-diffusion coefficients. Muhr and Blanshard[32] outline several effects that contribute to the decrease in self-diffusion coefficients from the bulk solvent values to those for imbibed solvents. The obstruction effect, which is the additional distance traveled by the solvent because of the presence of the polymer, accounts for the differences between the bulk and imbibed methanol self-diffusion coefficients but does not account for the differences within the polymer.

Blum et al.[33-36] have studied the self-diffusion coefficients of small molecules in polymer solutions and have shown that the polymer segmental mobility plays an important role in decreasing the solvent self-diffusion coefficients because of the polymer's restricted ability to move from the path of an oncoming solvent molecule. They also demonstrate that a surfce can exert a frictional effect on solvent mobility out to a few monolayers of solvent.

The decreasing self-diffusion coefficients can be explained by extending Blum et al.[34] to an anisotropic sample where one region of the polymer is swollen and the other has no solvent intrusion. Since the interface between the two regions is sharp for Case II diffusion, it is effectively a surface and exerts a frictional effect on the solvent molecules in the vicinity. However, the change in diffusion rates occurs over a much larger region than would be influenced by the surface effect alone.

The polymer segmental mobility dominates the decrease in solvent mobility. The polymer molecular motions in the glass are severely restricted compared to those in the swollen region. Since the sharp front exists, the polymer chains associated with both regions must be considered anchored at the interface between the swollen and the glassy regions. On the swollen side of the interface, one end of the chain is fixed and the remainder of the chain is free to move so that the motions of the chains decrease toward the interface. The rigidity of the polymer chains in the swollen region near the glass hinders the solvent mobility reducing the solvent self-diffusion coefficient.

Acetone swells PMMA to a greater extent than methanol. The self-diffusion coefficient image in Figure 14 shows several features caused by the increased activity and consequently the increased solvent volume fraction. The self-diffusion coefficients of the system are about 2 orders of magnitude greater than those of the methanol/PMMA system. This is clearly due to the increased volume available to the acetone molecules. The static obstructions (i.e. the polymer chains) decrease from 75% (volume) in the methanol case to 5% in the acetone system. The dynamic obstruction effect also decreases but is still evident in Figure 14. The self-diffusion coefficients of the system decrease by 35% from equilibrium to the region near the glassy core. The decreasing motions of the polymer chains as the core is approached reduces the solvent mobility in the same fashion as they did in the methanol case. But, the increased activity imparts more motions on the polymer chains in the acetone case so that the effective self-diffusion coefficient near the surface is 2 orders of magnitude greater than in the methanol system.

The glassy core influences the solvent behavior in the region bound by the glassy core and the area where the self-diffusion coefficients become constant as shown in Figure 14. The remainder of the swollen region has reached an equilibrium mobility for the solvent and the polymer and thus has a constant self-diffusion coefficient. Several factors contribute to the determination of this distance including the temperature, the solvent activity, and the polymer molecular weight. Further work is needed to determine the extent of each of these factors.

The currently postulated Case II theories make assumptions concerning the solvent diffusion in the swollen region. Thomas and Windle[17] assume that the diffusivity, D, increases exponentially with methanol concentration until an equilibrium value is reached. Hui et al.[18,19] assume that the solvent diffusivity in the rubber, D_r, is so much greater than that in the glass, D_g, that the ratio is considered to be infinite.

The range of solvent self-diffusion coefficients measured is from 10^{-5} to 10^{-8} cm^2 s^{-1}. This is 5 or 6 orders of magnitude larger than Hui et al. calculated for D_g (1×10^{-13} cm^2 s^{-1}) for diffusion of iodohexane into polystyrene. So their assumption seems valid. However, the decrease in solvent self-diffusion coefficients indicates that the slope of the diffusivity profile may be less steep than previously thought.

Comparison of Methods. The T_1s and T_2s are each measured by using two different techniques. In both cases the series method has a greater standard deviation than the more specific sequence. T_2s by the series method suffer from two deficiencies. Each image from a different echo time is collected at a different time. The total elapsed time from the first image to the last is long depending on the number collected. In that time, the interface between the glassy core and the swollen region may move significantly.[16] The sample may change its physical position slightly due to mechanical vibrations. These factors contribute to misregistration between the different images and cause the fitting routines to produce larger errors. The solvent self-diffusion also causes attenuation of the signal during long echo times adding additional losses.[20] The multiecho sequence does not suffer from these problems because signals from all of the echo times are collected successively during each phase encoding step of the imaging sequence. All of the images are acquired in the time normally required to collect one image. Also since the echoes are acquired rapidly, no attenuation occurs from self-diffusion.

The T_1s measured by the two different methods are considerably different. The data from the partial saturation method are probably skewed toward longer values because the TRs were longer than the T_1s. The T_1 inversion recovery experiment is more sensitive than the series method because it is directly measuring the relaxation process rather than the saturation process measured by the series method. It is also more sensitive visually because the data are presented in a phase-sensitive mode rather than a magnitude mode. The contrast is enhanced because the real difference between intensities is greater than the differences between the absolute value of the intensities.

Two pulse sequences are available to generate self-diffusion coefficient images, the spin-echo technique and the stimulated-echo technique. The stimulated-echo pulse sequence was used in this investigation because of its ability to store magnetization along H_0 so that T_2 relaxation is minimized. The stimulated-echo technique provides the ability to look at solvents with small self-diffusion coefficients with short T_2s whereas the spin-echo sequence permits study of solvents with longer T_2s.

Conclusion

NMR imaging has proven useful for probing the molecular dynamics of polymer/solvent systems exhibiting Case II diffusion. The solvent dynamics are indicative of the motions of the polymer chains in the swollen region because of the physical interaction of the solvent with the polymer. The mobility of the solvent and the polymer chains decreases toward the glassy core. The decreases in both the long- and short-range motions represent a mobility gradient that occurs when one end of the polymer is fixed and the other end is relatively free. From this information, it is apparent that the mobility of the solvent near the glass–rubber interface is different from the remainder of the imbibed or bulk solvent and should be considered in the current Case II theories.[17-19]

While Case II diffusion is characterized by a sharp front and constant solvent concentration in the swollen regions, it is clear from these NMR images that the molecular dynamics of the process are not as well understood. The decreases in solvent self-diffusion coefficients result from the influence of the polymer motions on the solvent mobility. Since the polymer chains are effectively fixed at the glass–rubber interface, the polymer segmental mobility decreases toward the interface as reflected by the solvent self-diffusion coefficients. The acetone/PMMA data indicate that the solvent activity influences the distance from the core where an equilibrium motional state is reached. Other influences on this distance include polymer molecular weight and temperature.

The magnitude of the self-diffusion coefficients supports current Case II theories that assume the solvent diffusivity is much higher in the swollen regions than in the glass. However, the spatial distributions of solvent self-diffusion coefficients indicate that the change in diffusivity is more gradual than assumed in current theories.

Several imaging techniques are demonstrated for measuring NMR relaxation parameters of solvents in polymers. The methods that measure the parameters quickly and directly provide the best results especially when considering a dynamic system such as diffusion in a polymer.

Acknowledgment. We wish to thank the National Science Foundation for its support through the Materials Research Grant at Case Western Reserve University. We also with to thank Dr. Juwhan Liu for his assistance with the computer simulations and data processing.

References and Notes

(1) Andrew, E. R. *Acc. Chem. Rev.* **1983**, *16*, 114.
(2) Budinger, T. F.; Lauterbur, P. C. *Science* **1984**, *226*, 288.
(3) Bailes, D. R.; Bryant, D. J. *Contemp. Phys.* **1984**, *24*, 441.
(4) Smith, S. L. *Anal. Chem.* **1985**, *57*, 595A.
(5) Pykett, I. L. *Sci. Am.* **1982**, *246*, 78.
(6) Luiten, A. L. *Essentials of Clinical MRI*; Falke, T. H. M., Ed.; Martinus Nijhoff Publishers: Boston, 1988; p 3.
(7) Rothwell, W. P.; Gentempo, P. P. *Bruker Report* **1985**, *1*, 46.
(8) Yamamoto, E.; Kohno, H. *IEEE Transactions on Medical Imaging* **1986**, *MI-5*, 229.
(9) Brown, T. R.; Kincaid, B. M.; Ugurbil, K. *Proc. Natl. Acad. Sci. U.S.A.* **1982**, *79*, 3523.
(10) Brateman, L. *Am. J. Rad.* **1986**, *146*, 971.
(11) Rothwell, W. P.; Holecek, D. R.; Kershaw, J. A. *J. Polym. Sci., Polym. Lett. Ed.* **1984**, *22*, 241.
(12) Rothwell, W. P.; Vinegar, H. J. *Appl. Opt.* **1985**, *24*, 3972.
(13) Blackband, S.; Mansfield, P. *J. Phys. C: Solid State Phys.* **1986**, *19*, L49.
(14) Weisenberger, L. A.; Koenig, J. L. *J. Polym. Sci. Polym. Lett. Ed.*, **1989**, *27*, 55.
(15) Weisenberger, L. A.; Koenig, J. L. *Polym. Prepr. (Am. Chem. Soc., Div. Polym. Chem.)* **1988**, *29*, 98.
(16) Weisenberger, L. A.; Koenig, J. L. *Appl. Spectrosc.* **1989**, *43*, 1117.
(17) Thomas, N. L.; Windle, A. H. *Polymer* **1982**, *23*, 529.
(18) Hui, C.-Y.; Wu. K.-C.; Lasky, R. C.; Kramer, E. J. *J. Appl. Phys.* **1987**, *61*, 5129.
(19) Hui, C.-Y.; Wu, K.-C.; Lasky, R. C.; Kramer, E. J. *J. Appl. Phys.* **1987**, *61*, 5137.
(20) Carr, H. Y.; Purcell, E. M. *Phys. Rev.* **1954**, *94*, 630.
(21) Meiboom, S.; Gill, D. *Rev. Sci. Instrum.* **1958**, *29*, 688.
(22) Stejskal, E. O.; Tanner, J. E. *J. Chem. Phys.* **1965**, *42*, 288.
(23) Le Bihan, D.; Breton, E.; Lallemand, D.; Grenier, P.; Cabanis, E.; Laval-Jeantet, M. *Radiology* **1986**, *161*, 401.
(24) Merboldt, K.-D.; Hänicke, W.; Frahm, J. *J. Magn. Reson.* **1985**, *64*, 479.
(25) Sattin, W.; Mareci, T. H.; Scott, K. N. *J. Magn. Reson.* **1985**, *65*, 298.
(26) Tanner, J. E. *J. Chem. Phys.* **1970**, *52*, 2523.
(27) Alfrey, T. *Chem. Eng. News* **1965**, *43*, 64.
(28) Thomas, N. L.; Windle, A. H. *Polymer* **1977**, *18*, 1195.
(29) Thomas, N. L.; Windle, A. H. *Polymer* **1978**, *19*, 255.
(30) Thomas, N. L.; Windle, A. H. *Polymer* **1981**, *22*, 627.
(31) Valsamidis, K.; Weisenberger, L. A.; Koenig, J. Unpublished infrared spectroscopic data.
(32) Muhr, A. H.; Blanshard, J. M. V. *Polymer* **1982**, *23*, 1012.
(33) Blum, F. D.; Pickup, S.; Foster, K. R. *J. Colloid Interface Sci.* **1986**, *113*, 336.
(34) Blum, F. D.; Durairaj, B.; Padmanabhan, A. S. *J. Polym. Sci., Polym. Phys. Ed.* **1986**, *24*, 493.
(35) Pickup, S.; Blum, F. D.; Ford, W. T.; Periyasamy, M. *J. Am. Chem. Soc.* **1986**, *108*, 3987.
(36) Ford, W. T.; Ackerson, B. J.; Blum, F. D.; Periyasamy, M.; Pickup, S. *J. Am. Chem. Soc.* **1987**, *109*, 7276.